Reversible Wetting−Dewetting Transitions on Electrically Tunable Superhydrophobic Nanostructured Surfaces

Tom N. Krupenkin,* J. Ashley Taylor, Evelyn N. Wang, Paul Kolodner, Marc Hodes, and Todd R. Salamon

Bell Laboratories, Alcatel-Lucent, Murray Hill, New Jersey 07974

Received March 23, 2007. In Final Form: May 25, 2007

In this work, electrically controlled fully reversible wetting−dewetting transitions on superhydrophobic nanostructured surfaces have been demonstrated. Droplet behavior can be reversibly switched between the superhydrophobic Cassie−Baxter state and the hydrophilic Wenzel state by the application of electrical voltage and current. The nature of the reversibility mechanism was studied both experimentally and theoretically. The reported results can provide a new method of dynamically controlling liquid−solid interactions.

Introduction

Superhydrophobic surfaces have attracted substantial interest from academic and industrial research communities over the past decade because of their interesting and unusual interfacial properties, including extremely high contact angles, very low flow resistance, and the ability to self-clean.[1−10] These properties make superhydrophobic surfaces important candidates for a wide range of applications, from microfluidics and lab-on-a-chip devices to drag reduction and liquid-based cooling of microelectronics. In many of these applications, it would be highly advantageous to dynamically control the interaction of liquids with the superhydrophobic surface, including the modification of the contact angle, droplet mobility, and degree of penetration of liquid into the superhydrophobic surface. Although several approaches to achieving dynamic tuning of the wetting behavior of unstructured surfaces have been known for some time,[11−13] only recently have the first successful attempts demonstrating effective dynamic tuning of superhydrophobic surfaces been reported.[14−16] In particular, in ref 14 a method that allows dynamic electrical control of the whole range of wetting behavior (from hydrophilic to superhydrophobic behavior) of liquids on nanostructured surfaces has been demonstrated. Although this approach shows substantial promise for potential applications, it suffers an important shortcoming—the transition from superhydrophobic to hydrophilic behavior is not reversible. Later,[16] it was shown that this transition can be reversed by the application of electrical current. However, the need for a detailed investigation of the mechanism of the reversibility remained. In the present work, the physical mechanism of the fully reversible, electrically controlled wetting-to-dewetting transitions on superhydrophobic nanostructured surfaces is investigated. Droplet behavior is shown to be reversibly switched between the superhydrophobic Cassie−Baxter state and the hydrophilic Wenzel state by the application of electrical voltage and current. The results provide a new method of dynamically controlling liquid−solid interaction. This ability to switch the surface reversibly between superhydrophobic and hydrophilic states substantially broadens the applicability of tunable nanostructured surfaces.

Superhydrophobic surfaces utilize a combination of surface roughness and surface chemical treatment to enhance the hydrophobicity of a surface. Droplets placed on such surfaces often reside in one of two states: the so-called Cassie−Baxter state,[17] where the droplet rests on top of the surface roughness features and a layer of air is present below the droplet within the superhydrophobic surface, and the so-called Wenzel state,[18] where the fluid completely wets the surface roughness features. A large body of work has examined how fluids interact with surfaces having different roughness characteristics and chemical composition.[2,8−10,17−19] Of particular relevance to this letter is the work of He et al.,[19] who showed the existence of metastable states on a surface consisting of square pillars of polydimethylsiloxane, where it was energetically unfavorable to transition, for example, from the Cassie−Baxter state to a lower-energy Wenzel state. Developing methods for controlling transitions between stable and metastable states on superhydrophobic surfaces is crucial for dynamically tuning the properties of these novel materials.

In this letter, we use electrowetting, where a potential difference is applied between the droplet and the underlying substrate, to induce a transition from a superhydrophobic state to a hydrophilic state where the fluid wets the superhydrophobic surface roughness features. The applied potential difference results in a modification to the solid/liquid interfacial energy, which causes the droplet to spread so as to minimize the total energy of the system. The droplet remains in its wetted state upon removal of the applied potential difference, even though the wetted state is no longer

* Corresponding author. E-mail: tnk@alcatel-lucent.com.

(1) Shibuichi, S.; Onda, T.; Satoh, N.; Tsujii, K. *J. Phys. Chem.* **1996**, *100*, 19512.
(2) Miwa, M.; Nacajima, A.; Fujishima, A.; Hashimoto, K.; Watanabe, T. *Langmuir* **2000**, *16*, 5754.
(3) Chen, W.; Fadeev, A.; Hsieh, M. C.; Oner, D.; Youngblood, J.; McCarthy, T. J. *Langmuir* **1999**, *15*, 3395.
(4) Youngblood, J. P.; McCarthy, T. J. *Macromolecules* **1999**, *32*, 6800.
(5) Inoue, Y.; Yoshimura, Y.; Ikeda, Y.; Kohno, A. *Colloids Surf., B* **2000**, *19*, 257.
(6) Matsumoto, Y.; Ishida, M. *Sens. Actuators* **2000**, *83*, 179.
(7) Hozumi, A.; Takai, O. *Thin Solid Films* **1997**, *303*, 222.
(8) Bico, J.; Marzolin, C.; Quere, D. *Europhys. Lett.* **1999**, *47*, 220.
(9) Nakejima, A.; Hashimoto, K.; Watanabe, T. *Monatsh. Chem.* **2001**, *132*, 31.
(10) Lafuma, A.; Quere, D. *Nat. Mater.* **2003**, *2*, 457.
(11) Ichimura, K.; Oh, S.-K.; Nakagawa, M. *Science* **2000**, *288*, 1624.
(12) Lahann, J.; Mitragotri, S.; Tran, T.-N.; Kaido, H.; Sundaram, J.; Choi, I. S.; Hoffer, S.; Somorjai, G.; Langer, R. *Science* **2003**, *299*, 371.
(13) Isaakson, J.; Tengstedt, C.; Fahlman, M.; Robinson, N.; Berggren, M. *Adv. Mater.* **2004**, *16*, 316.
(14) Krupenkin, T.; Taylor, J.; Schneider, T.; Yang, S. *Langmuir* **2004**, *20*, 3824.
(15) Sun, T.; Wang, G.; Feng, L.; Liu, B.; Ma, Y.; Jiang, L.; Zhu, D. *Angew. Chem.* **2004**, *43*, 357.
(16) Krupenkin, T.; Taylor, J. A.; Kolodner, P.; Hodes, M. *Bell Labs Techn. J.* **2005**, *10*, 161.
(17) Cassie, A. B. D.; Baxter, S. *Trans. Faraday Soc.* **1944**, *40*, 546.
(18) Wenzel, R. N. *J. Phys. Colloid Chem.* **1949**, *53*, 1446.
(19) He, B. H.; Patankar, N. A.; Lee, J. *Langmuir* **2003**, *19*, 4999.

10.1021/la7008557 CCC: $37.00
Published on Web 07/31/2007

the minimum-energy state when the voltage is removed. In this sense, the described above transition is irreversible.

The details of the physical mechanisms that make the initial electrowetting-induced transition on nanostructured surfaces irreversible require additional investigation, but one fact is clear: the transition involves sizable energy dissipation associated with the propagation of the liquid front through the nanostructured layer during the wetting process. As a result, the droplet contact line becomes effectively pinned, and the transition becomes irreversible because the system lacks the energy necessary to move the droplet contact line back to the initial position when the voltage is removed.

On the basis of the aforementioned observation, one can conceive of two general approaches to make the transition reversible: (i) engineer the morphology of the nanostructured layer in such a way as to minimize the undesirable energy dissipation and thereby reduce or eliminate the energy barrier for transitioning to the lower-energy superhydrophobic state or (ii) provide additional energy to the system in order to reverse the transition. Both of these approaches potentially have their own problems and advantages. The specially engineered nanostructured surfaces would require substantially reduced energy or no energy to reverse the transition but might suffer from substantial restrictions on the morphologies that can be used, thus potentially impeding their performance. However, if one can develop an effective way to provide additional energy to the system to facilitate the reverse transition, the resulting mechanism might be rather general and would work for a wide variety of nanostructure morphologies. The potential drawback in this case is developing a robust, efficient mode of energy transfer that drives the system toward the original superhydrophobic configuration.

One way to provide extra energy to the system and initiate a reverse transition is to generate a very thin layer of vapor or gas adjacent to the substrate surface. As the thickness of the vapor layer becomes comparable to the thickness of the nanostructured layer, the liquid effectively disconnects from the surface of the nanostructured substrate, thereby eliminating contact line pinning, and the system returns to the initial superhydrophobic state. This approach can be especially effective in the case of closed-cell nanostructures, such as the "nanobricks" described below in the Experimental Section, where a layer of air can be trapped at the bottom of each cell during the initial electrowetting-induced transition. Momentarily increasing the temperature of the substrate surface in such a system will temporarily increase the volume occupied by the trapped gas and vapor and will thus initiate the reverse transition.

In this respect, two limiting cases could be considered. In the first case, most of the volume change is provided by the trapped air, such as for the closed-cell structures described above. In the second case, most of the volume change is provided by the vapor. In this configuration, there may be no air trapped next to the substrate, and all of the vapor is produced directly at the liquid−substrate interface during the temperature increase. The latter case is potentially the more effective one and would be expected to work for both closed-cell and open-cell structures, provided enough vapor is produced.

Experimental Section

The purpose of this work is to investigate a particular case of thermally induced reversible transitions in which no air is trapped and the droplet disconnects from the nanostructured surface by a vapor layer produced during the transition process. In this case, the transition is induced by a rapid but temporary increase in the sample surface temperature.

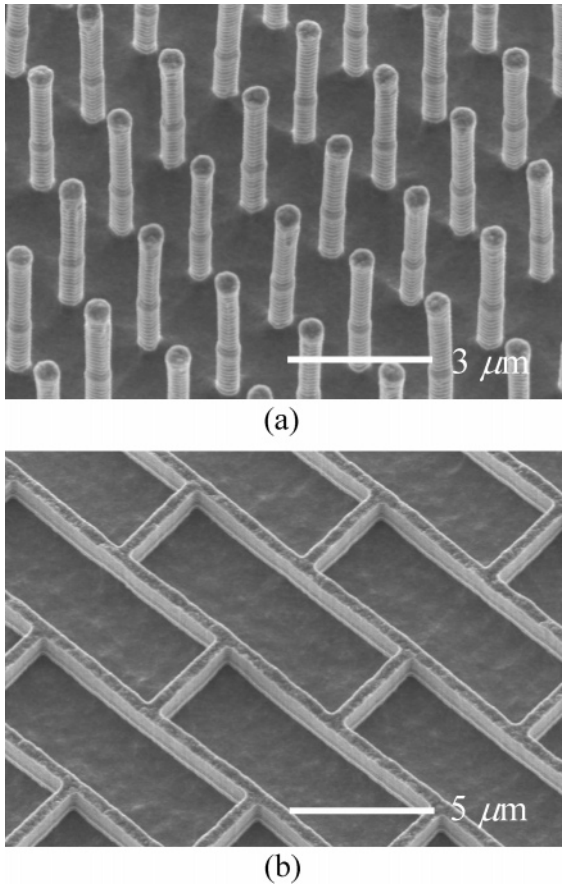

Figure 1. Scanning electron micrographs of the nanostructured substrates used in this work. (a) Nanograss substrate. Each nanopost is about 4.8 μm tall and has a diameter of about 500 nm. The distance between the centers of the posts is 2 μm. (b) Nanobrick substrate. Each nanobrick cell is 4 μm wide $\times$ 10 μm long. The walls separating the cells are 1.7 μm tall and have a thickness of about 500 nm.

Two types of nanostructured substrates were investigated in this work: "nanograss" (Figure 1a), which represents an open-cell structure, and "nanobricks" (Figure 1b), which represent an example of a closed-cell structure. Both substrates were produced by reactive ion etching of a nanopattern into the surface of a custom-made silicon-on-insulator wafer. The nanostructures were formed on top of a 7.4-μm-thick, highly conductive, phosphorus-doped polysilicon layer that was electrically isolated from the rest of the wafer by a thin underlying thermal oxide layer. Thermal oxide was grown on the silicon posts, and then a thin conformal layer of a low-surface-energy polymer was deposited to create the hydrophobic surface. The Materials and Methods section available in Supporting Information contains a detailed description of the substrates and how they were fabricated.

The typical experimental procedure employed to study the reversible transition involved two major steps. First, the droplet was positioned on top of the nanostructured substrate. The liquid remained suspended at the top of the nanostructured layer and formed a highly mobile "rolling ball" state at this stage. Then the electrowetting-induced transition from the superhydrophobic rolling ball state to the hydrophilic, immobile droplet state was initiated by applying a voltage between the droplet and the conductive top layer of the substrate. The liquid penetrated all the way to the bottom of the nanostructured layer as a result of this transition. Note that electrowetting-induced transitions on nanostructured surfaces have been studied previously and are described in detail in ref 14.

In the second step, a short pulse of electrical current provided by a capacitor discharge was transmitted through the highly conductive top layer of the substrate, causing a momentary increase in the surface temperature of the sample and the formation of a thin layer of vapor at the liquid−solid interface. As a result of the capacitor discharge,

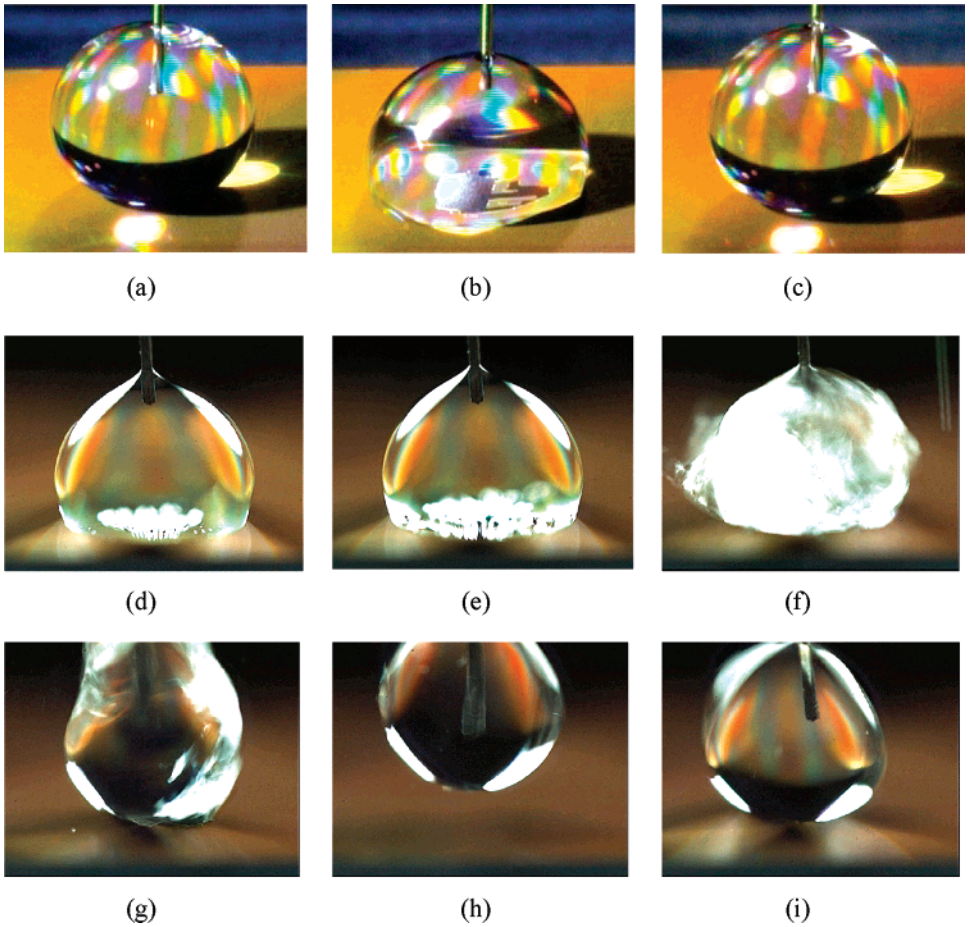

Figure 2. Demonstration of electrically induced reversible transitions between different wetting states of a liquid on a nanostructured substrate. To induce a transition between a rolling ball and an immobile droplet, a voltage was applied between the droplet (contacted through a Pt wire) and the substrate. To reverse the transition and convert the immobile droplet back to the rolling ball state, a short pulse of electrical current was transmitted through the highly conductive 7.4 μm surface layer of the substrate. (a) With no voltage applied, a water droplet formed a highly mobile rolling ball on the nanograss substrate. (b) With the application of about 35 V, the water droplet on the nanograss substrate underwent a sharp transition to the immobile droplet state. (c) After a short pulse of electrical current was transmitted through the nanograss substrate, the droplet returned to the original rolling ball state. High-speed video recordings of the hydrophilic−superhydrophobic transition of a 10 μL droplet were obtained using a pulse energy of 30 J/cm^2. (d) At $t = 0$, the electrical pulse is applied to the immobile droplet. A few trapped air bubbles are visible at the bottom of the droplet. (e) At $t = 17$ ms, multiple vapor bubbles appear at the liquid−solid interface. (f) At $t = 26$ ms, the footprint of the droplet starts to shrink. (g) At $t = 31$ ms, the droplet disconnects from the substrate. (h) At $t = 40$ ms, the inertia of the droplet propels it to its maximum height. (i) At $t = 50$ ms, the droplet lands back on the substrate and returns back to its superhydrophobic state.

the droplet disconnected from the substrate surface and returned to the superhydrophobic rolling ball state, thus reversing the initial electrowetting transition. In the majority of experiments, we used water with a small amount of $ZnCl_2$ added to increase the electrical conductivity. The details of the experimental procedure, along with the materials and equipment used, are described in detail in the Materials and Methods section available in Supporting Information.

Typical results obtained with this experimental procedure for water droplets are shown in Figure 2a−c. With no voltage applied, the droplets formed a very mobile ball (Figure 2a). When 35 V was applied, the droplet underwent a sharp transition to the immobile droplet state (Figure 2b). After a short pulse of electrical current was transmitted through the substrate, the droplet then returned to the original rolling ball state (Figure 2c).

To further elucidate the dynamics of the hydrophilic−superhydrophobic transition, high-speed video recording of the transition process was performed with a 10 μL droplet. Typical results are shown in Figure 2d−i. Three distinct stages of the transition can be clearly observed. First, about 17 ms from the beginning of the pulse, multiple vapor bubbles appear at the liquid−solid interface at the bottom of the droplet (Figure 2e). As the temperature of the substrate continues to rise, a violent boiling process develops, and about 26 ms from the beginning of the pulse, the droplet footprint begins to shrink (Figure 2f). The footprint shrinkage continues for about 5 ms and ends when the droplet completely disconnects from the substrate and returns to the initial superhydrophobic state (Figure 2g).

It is interesting that the inertia of the droplet is sufficient to propel the droplet several hundred micrometers up in the air, as shown in Figure 2h. The other important point is that, once disconnected, the droplet remains in the superhydrophobic rolling ball state and does not penetrate the nanostructured layer. This is illustrated in Figure 2i, which shows the droplet after it lands back on the substrate. One can see that no boiling is observed at the liquid−solid interface at the bottom of the droplet.

To obtain a better understanding of the physical mechanism responsible for the droplet returning to the rolling ball state, the reversibility of the transition was studied as a function of the electrical pulse energy and characteristic pulse duration time. The results are shown in Figure 3 for the nanograss substrate. It can be seen that the main parameter governing the transition reversibility is the total pulse energy delivered per unit area of the sample. It appears that the duration of the pulse has little effect on the transition reversibility, at least for the pulse durations investigated in the current work that range from approximately 20 to 60 ms. Similar results were obtained for the nanobrick substrate and are available in the Supporting Information. To achieve the transition, a cumulative energy in excess

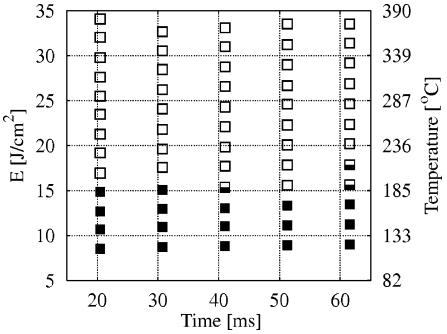

Figure 3. Transition reversibility map for water droplets on a nanograss substrate. The vertical axes represent the applied electrical pulse energy per unit area of the sample surface (left) and the maximum sample surface temperature (right). The horizontal axis represents the characteristic duration of the pulse. Filled squares correspond to the cases where no reversibility was achieved, empty squares correspond to the case where reversibility was always achieved, and half-filled squares correspond to the cases with about 50% probability of reversing the transition.

of about 15 J/cm^2 for the nanograss substrate and about 14 J/cm^2 for the nanobrick substrate must be deposited, irrespective of the pulse duration.

Further insight into the physics of the reversibility phenomenon is provided by temperature measurements. From these measurements, we find that the reversibility of the transition is correlated with the maximum sample surface temperature (which scales with the total pulse energy) and not with the maximum heat flux produced by the sample (which scales with the pulse energy divided by the pulse duration).

To this end, three complementary experimental techniques were used to determine the thermal behavior of the sample. First, the temperature at the center of the underside of the sample was measured by a thermocouple. Because of the relatively large thermal inertia of the thermocouple, this method was suitable for recording the sample temperatures only at times longer than about 1 s (i.e., well after the end of the pulse). Second, an infrared camera was used to determine the temperature distribution of the sample surface as a function of time. This method provided 16 ms time resolution and very good spatial resolution (with 115 μm pixel size). Finally, the average surface temperature of the sample during the pulse itself (i.e., in the first ~200 ms) was determined from the relative change in electrical resistance of the highly conductive top layer of the substrate. This approach provided the best temporal resolution (better then 1 ms). Because this method requires a flow of electrical current through the sample, the measurement error progressively increases with time as the pulse current diminishes.

The results obtained by all three techniques were in good agreement. Typical results of the infrared camera measurements are shown in Figure 4a−c using the nanograss substrate as an example. One can see that the surface temperature of the sample quickly reaches saturation and then remains largely constant for a long time (Figure 4b). This indicates that the sample cooling mechanisms (air convection, radiation cooling, thermal conduction to the sample support structure, etc.) are relatively weak and can be neglected at times comparable to the electrical pulse duration. The temperature distribution along the sample is shown in Figure 4c. One can see that, although the ends of the sample are colder than the center, the overall temperature variation along the central two-thirds of the sample length is not very substantial. Details of the temperature measurement procedure are available in the Materials and Methods section in Supporting Information.

Knowledge of the temperature of the interface between the sample and the droplet is particularly important because it determines the liquid evaporation process. To supplement the data obtained by the experimental measurements, direct numerical modeling of the sample temperature evolution was performed. The modeling was performed using FIDAP, a finite-element-based software package for simulating heat transport and fluid flow. The sample was modeled as a silicon

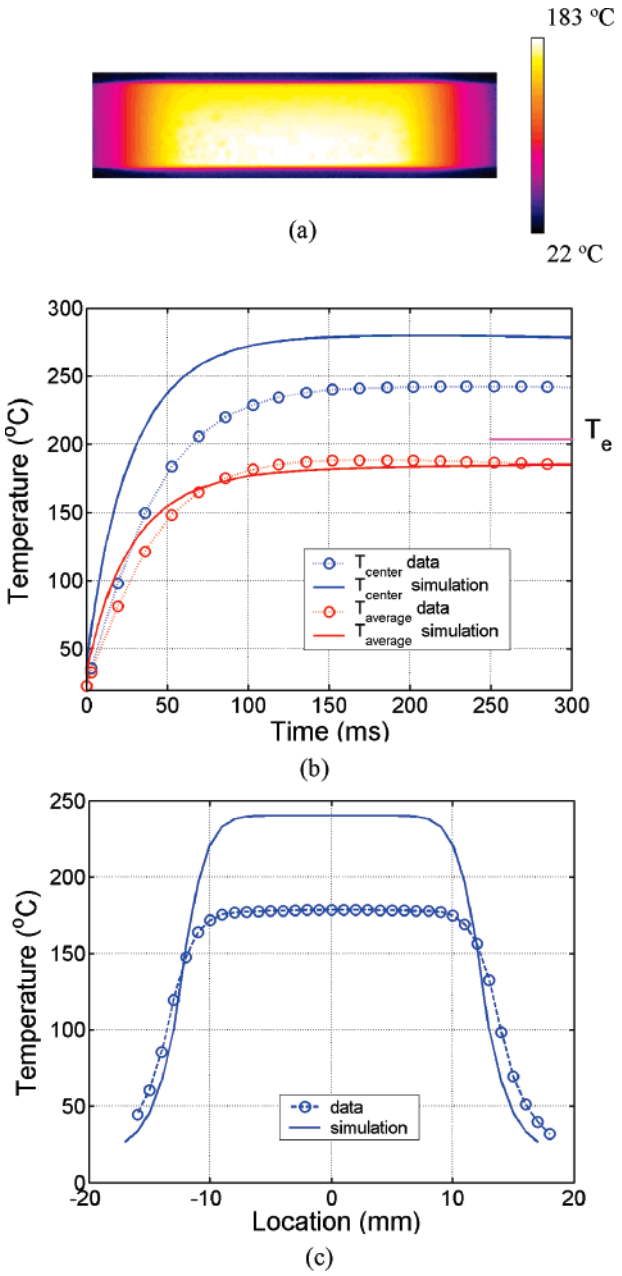

Figure 4. Temperature distributions of the nanograss substrate during a short electrical pulse obtained from infrared camera measurements and FIDAP simulations. The pulse energy used was 22 J/cm^2, and the pulse characteristic time was 31 ms. (a) An example infrared image obtained at 56 ms from the beginning of the electrical pulse. (b) Average (shown in red) and center temperature (shown in blue) of the substrate as a function of time. The circles correspond to the infrared measurements, and the lines correspond to numerical modeling results. T_e is the calculated bulk temperature of the substrate when the energy provided by the pulse is used to heat the substrate uniformly without any losses. (c) Temperature profile of the substrate 56 ms from the beginning of the electrical pulse. Location 0 mm is the center of the chip. The circles correspond to infrared measurements, and the lines correspond to numerical modeling results.

plate with an infinitesimally thin heater located on its top surface and covering approximately two-thirds of the sample area. The time-varying energy dissipated by the heater was determined from the pulse current. The surface temperature was computed as a function of time at a number of points along the sample surface. The details of the model and the assumed material properties are described in the Numerical Modeling section in Supporting Information. The simulated results, shown in Figure 4b,c, are in reasonable agreement

with the experimental measurements discussed above. The model accurately predicts the average sample temperature but overestimates the temperature rise at the center of the sample by between 10% (at long times) and 25% (at short times). This is not unexpected because the model assumes that all of the heat is generated at the central two-thirds of the sample whereas in the actual experiment some of the heat was generated at the sample ends as well. In addition, the model does not take into account the heat losses from the support structure, solder bumps, and wire leads.

Knowledge of the sample temperature evolution, coupled with information about the droplet transition dynamics obtained from high-speed video recording, can shed additional light on the physics of the reversibility process.

Discussion

As shown in the previous section, the main parameter that governs the hydrophilic−superhydrophobic transition is the total energy per unit area of the sample delivered by the electrical pulse. This can be further supported by combining the transition reversibility map with the temperature measurement data. The result is shown on the right vertical axis in Figure 3, where the maximum temperature at the center of the sample is correlated with the electrical pulse energy. From these results, one can infer that the reverse (i.e., dewetting) transition occurs when the maximum surface temperature of the sample exceeds critical temperatures of about 190 °C for the nanograss samples and about 180 °C for the nanobrick samples. It is important to note that these critical temperatures are well above the boiling point of water.

Further insight into the dynamics of the reversibility process can be obtained by correlating the dewetting transition stages recorded by the high-speed video camera with the sample surface temperature. The results are presented in Figure 5a, where the time required to reach a certain transition stage (i.e., vapor bubble nucleation, droplet footprint shrinkage, and droplet disconnect) is compared to the time by which the sample surface reaches certain specific temperatures. It can be seen that there is good correlation between the timing of the transition stages and the sample surface temperature. Thus, the first vapor bubbles appear when the sample temperature reaches about 100 °C. Droplet footprint shrinkage starts at a temperature of about 130 °C. Finally, the droplet disconnects at a temperature of about 190 °C. One can also observe that if the total pulse energy is not sufficient to achieve the critical surface temperature of 190 °C the droplet footprint shrinkage stage is never completed, thus preventing the droplet from disconnecting and returning to the superhydrophobic state.

The obtained transition temperatures are in good agreement with the characteristic temperatures associated with different stages of boiling.[20] Bubble formation starts at 100 °C, as expected for nucleate boiling of water. Droplet footprint shrinkage begins at about 130 °C, which corresponds to the transition from nucleate to mixed boiling, and droplet disconnect happens around 190 °C, close to where the transition to film boiling is expected to occur. This supports the notion that the droplet undergoes a reverse transition when it becomes completely disconnected from the substrate by a vapor layer as the film boiling stage is reached.[20]

During the footprint shrinkage process, the droplet shape becomes progressively more rounded under the influence of the surface tension force. As a result, the center of mass of the droplet begins to move up, and the droplet acquires a certain amount of kinetic energy. Once the droplet is completely disconnected from the substrate, it is propelled up into the air, and its kinetic energy

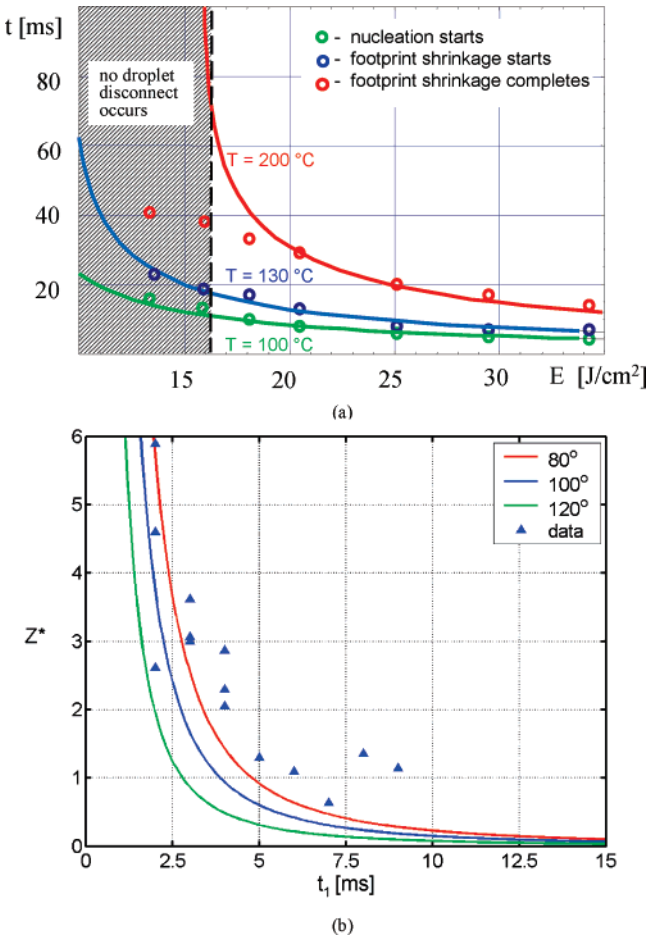

Figure 5. Droplet dynamics of the reversibility process. (a) Dewetting transition stages as a function of time and temperature. The plot was obtained by correlating the different stages recorded by a high-speed camera to sample surface temperature. There is good correlation between the timing of the transition stages and the surface temperature of the sample. Vapor bubbles first appear when the sample reaches about 100 °C, the droplet begins to shrink when the surface temperature reaches about 130 °C, and the droplet disconnects when the surface temperature reaches about 190 °C. These transition temperatures are in good agreement with characteristic temperatures associated with different stages of boiling. The pulse energies range from 13 to 34 J/cm^2, and the characteristic pulse time was 15 ms. (b) Normalized droplet jump height as a function of the droplet footprint shrinkage time (t_1). When the droplet disconnects from the surface, it is propelled into the air, where its kinetic energy is converted into potential energy. The symbols represent experimental data with pulse energies ranging from 27 to 37 J/cm^2. The lines are analytical results obtained as a function of varying initial droplet contact angle in its immobile state. The experimental data and analytical results are in good agreement and suggest that increasing pulse energy leads to higher droplet heights because of shorter footprint shrinkage times.

is converted into potential energy in the field of gravity. Thus, one can establish a simple analytical relationship between the time of the footprint shrinkage stage and the height that the droplet jumps as derived in Supporting Information. The results are shown in Figure 5b and demonstrate reasonably good agreement between the theoretical prediction and the experimental data. As one can expect, the shorter the footprint shrinkage stage (and, consequently, the higher the droplet disconnect speed is), the higher the droplet jumps. Theoretically, higher-energy pulses should lead to higher droplet jump heights as a result of shorter footprint shrinkage times. Experimental observations support this trend. However, additional factors such as substrate

(20) Incropera, F. P.; DeWitt, D. P. *Fundamentals of Heat and Mass Transfer*, 3rd ed.; John Wiley & Sons: New York, 1990.

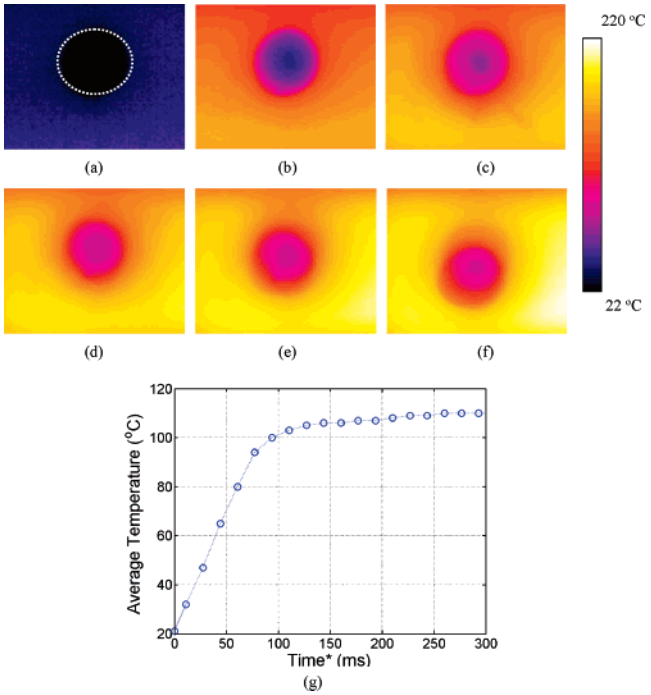

Figure 6. Temperature of the droplet during various stages of the reversible transition obtained from infrared camera measurements. The pulse energy used was 30 J/cm^2. (a) At $t = 0$, the electrical pulse is applied to the immobile droplet. The dotted white line outlines the location of the droplet. (b) At $t^* = 11$ ms, the droplet begins to heat up. (c) At $t^* = 27$ ms, the droplet is about to disconnect from the surface. (d) At $t^* = 44$ ms, the droplet is disconnected from the surface. (e) At $t^* = 61$ ms, the droplet heats up because of contact with the hot substrate. (f) At $t^* = 77$ ms, the droplet continues to heat up. (g) Average droplet temperature as a function of time (t^*). When the droplet disconnects, its bulk temperature reaches about 60 °C.

contamination and the particular position of the probe wire lead to scatter in the experimental data, as exemplified in Figure 5b.

The infrared imaging technique allows one to estimate the temperature of the droplet during various stages of the dewetting process. Typical experimental results are shown in Figure 6. At the moment of disconnect (Figure 6c), the droplet temperature reaches only about 60 °C (i.e., well below the boiling point of water). However, after the droplet lands back on the hot substrate, its temperature continues to rise and eventually reaches about 100 °C, as shown in Figure 6g. The resulting evaporation of the droplet leads to a decrease in its volume at a rate on the order of 0.1 μL/s. Because it took about 30 s for the droplet with a volume of 10−15 μL to cool down to room temperature in our experiments, the total loss of droplet volume was about 3 μL per transition. It should be noted that this loss happens primarily after the transition, while the droplet rests on a hot substrate. The loss of droplet volume during the transition itself is estimated to be below 0.5 μL. We expect that the total loss of droplet volume can be further decreased by minimizing the time that the substrate stays at high temperature. In particular, one can achieve rapid cooling of the substrate after the heat pulse by optimizing the substrate thermal conductivity and coupling it to an effective heat sink.

Conclusions

In this work, a new method of fully reversible dynamic electrical control of the wetting behavior of liquids on superhydrophobic nanostructured surfaces is proposed and experimentally demonstrated. The proposed approach allows reversible switching between superhydrophobic and hydrophilic behavior. The method employs electrowetting to induce the superhydrophobic-to-hydrophilic transition.[14] The transition is then reversed, and the system is returned back to the superhydrophobic state, when a short pulse of electrical current is transmitted through a thin, highly conductive surface layer of the sample, which causes a momentary evaporation of a microscopically thin layer of liquid immediately adjacent to the substrate surface. The proposed reversibility mechanism appears to be quite universal and has been demonstrated successfully on both open-cell and closed-cell nanostructures.

The dependence of the reversible transition was studied as a function of sample surface temperature and heat flux produced at the sample surface during the pulse. It was determined that the reversibility is governed primarily by the maximum sample surface temperature. The initial electrowetting transition is reversed when the sample surface temperature exceeds a certain critical value, which, for the case of water, was determined to be between 180 and 190 °C. At this temperature, a thin layer of liquid adjacent to the substrate undergoes a transition to the film boiling regime. As a result, the droplet disconnects from the substrate and returns to the initial superhydrophobic state.

The ability to electrically change the wetting behavior of solid surfaces from superhydrophobic to hydrophilic and back to superhydrophobic opens a wide range of exciting new applications. The work presented in this letter is the first to demonstrate a thermally based mechanism for reversing between wetting and nonwetting states on a superhydrophobic surface. Droplet-based microfluidics, fluidic drag reduction, liquid-based cooling of microelectronics, microbatteries, and chemical microreactors represent some of the areas that can potentially benefit from such technology.

Acknowledgment. Discussions with Joanna Aizenberg, Mary Mandich, and Alan Lyons are greatly appreciated. Also appreciated is the processing support of Stanley Pau, Ray Cirelli, and the New Jersey Nanotechnology Consortium. The help of Reja Amatya, a Lucent Global Scholar summer intern, is also greatly appreciated.

Supporting Information Available: Materials and methods and modeling. This material is available free of charge via the Internet at http://pubs.acs.org.

LA7008557